Journal of Civil and Hydraulic Engineering
https://www.acadlore.com/journals/JCHE

Numerical Analysis of Slope Stability in a Coal Mine Waste Dump Under Coupled Hydro-Mechanical-Thermal Influences: A Case Study of Maamba, Zambia

Lunenge Aggrey Lisulo[1*], Oscar Kamasongo[2], Kalaluka Kwalombota[3]

[1] College of Landscape Architecture, Zhejiang A & F University, 311300 Hangzhou, China
[2] School of Natural Sciences, Eden University, 10101 Lusaka, Zambia
[3] Department of Power Equipment, Technical University of Liberec, 46117 Liberec, Czech Republic

[*] Correspondence: Lunenge Aggrey Lisulo (lunengelisulo@gmail.com)

Received: 11-04-2024 **Revised:** 01-10-2025 **Accepted:** 03-07-2025

Citation: L. A. Lisulo, O. Kamasongo, and K. Kwalombota, "Numerical analysis of slope stability in a coal mine waste dump under coupled hydro-mechanical-thermal influences: A case study of Maamba, Zambia," *J. Civ. Hydraul. Eng.*, vol. 3, no. 2, pp. 56–76, 2025. https://doi.org/10.56578/jche030201.

Abstract: The instability of mining waste dumps poses significant environmental hazards, including loss of life, damage to infrastructure, and ecological degradation. The complex interdependence of Thermal, Hydraulic, and Mechanical (THM) processes has been increasingly recognised as a critical factor influencing slope stability. In this study, a coupled THM numerical model was developed using the finite element method (FEM) to evaluate slope stability in a coal mine waste dump in Maamba, Zambia. Key parameters, including stress distribution, displacement, pore water pressure, and temperature variations, were incorporated to achieve a comprehensive assessment of slope failure mechanisms. Field data and geotechnical investigations were integrated with advanced computational simulations to ensure realistic modelling. The findings demonstrated that conventional limit equilibrium methods (LEM) underestimated the impact of coupled processes on slope failure. The safety factor was observed to decrease by more than 30% due to THM interactions, with thermal gradients and hydro-mechanical (H-M) responses identified as primary contributors to slope instability. The results underscore the necessity of incorporating THM coupling in slope stability assessments, particularly in geotechnically sensitive mining environments. The proposed framework provides a scientifically grounded methodology for evaluating and mitigating landslide risks in mining waste dumps, offering valuable insights applicable to regions with similar geotechnical and climatic conditions. The findings contribute to the refinement of slope stability management strategies and provide a basis for the development of risk mitigation measures in vulnerable mining areas.

Keywords: Slope stability; Coupled Thermal, Hydraulic, and Mechanical (THM) effects; Finite element modelling (FEM); Numerical simulation; Mining waste dump; Landslide risk assessment

1 Introduction

Roadside landslides and open pit mines are common sites for landslide events, which can disrupt traffic and mining operations, respectively, and even result in casualties and property damage [1]. As a result, studying and analysing slope stability is important and meaningful and can yield important information for landslide prevention and early warning. Problems with unstable slopes can be caused by a variety of factors, including the formation of joints and fractures, surface drainage, groundwater conditions, human activities like excavation and climate change, and external factors like precipitation and seismic activity. Differences in the dimensions and geometry of the rock and soil mass. Also, exacerbate the problem [2, 3]. Rainfall-induced landslides are significantly more likely on mine waste dump slopes due to their loose and porous composition.

Due to a lack of available land for deposition, mine waste is usually stored in slopes or piles that progressively increase in height and size. These mine refuse dumps have long been a source of concern for mine site management [4, 5]. Thus, it is crucial to conduct additional research on the stability of mine waste dumps impacted by precipitation. The THM interaction (temperature variations brought on by seasonal changes) can have a substantial effect on slope stability [2]. Inadequate design of a mine waste dump can result in possible landslides, which can have immeasurable consequences such as casualties, property damage, and ecological degradation [6–8].

Slope stability has been evaluated recently, accounting for the coupled effects of H-M interactions. For example, looked into the basic causes of fill slope failures brought on by precipitation [9]. Precipitation can lead to slope failure because it drastically changes the ground surface flux boundary condition, decreasing the shear strength and effective stress of the soil. Furthermore, a few additional scholars have looked into slope stability within the framework of coupled H-M interactions [3, 10]. While fully coupled THM models for modelling the behaviour of geotechnical materials have been made available in several recent works, such as studies [4, 11–13]. They were not primarily concerned with slope-related problems.

Geotechnical hazards such as landslides affect the production processes in the open-pit mines, destroy mining facilities and infrastructure and are dangerous and potentially fatal to the workers. This makes it necessary to carry out a slope stability analysis to plan for early warning and possibly measures to prevent any occurrence. Several aspects, like joint formation, inadequate drainage, and water table oscillations, cause it. In addition to rainfall, mine waste slopes are vulnerable mainly because their ground comprises loose particles with low cohesiveness [14].

In the open slopes sited for mine waste storage, H-M interactions pose additional risks, mainly in precipitation, where the shear strength of the soil decreases and pore pressure rises. Both these coupled effects not only reduce safety factors but also exponentially increase the possibility of catastrophic slope failure [15]. Further development of these H-M dynamics is crucial for improving existing approaches to analysing the stability of slopes and identifying potential risks, as well as designing appropriate concepts and methods for landslide protection in mining conditions.

Table 1. A brief synopsis of the case studies

Author(s), Year	Applied Method	Landslide Measures	Major Findings
Schmertmann [16]	Numerical analysis method	None	A number of variables, including the amount and duration of rainfall and the soil's permeability, can affect how stable the built slope is. The user mentions the slope angle and the existence of an impermeable or permeable underlayer.
Zhao et al. [17]	The numerical simulation method using FLAC2D and the limit equilibrium method	Introduced seven techniques for landslide aversion	Prolonged and intense rainfall significantly increases the likelihood of slope landslides occurring.
Song [18]	Numerical method via Geostudio's (SEEP/W, SLOPE/W)	None	Rainfall infiltration caused the wetting front to move downward, lowering the slope's safety factor.
Masoudian et al. [19]	FEM and Monte Carlo simulation through Abaqus software.	None	After 10 days of precipitation, the probability of failure rose sharply from negligible to nearly 100%. demonstrated that rainfall infiltration significantly affects unsaturated slope stability.
Wu et al. [2]	Utilised COMSOL Multiphysics to perform the numerical Finite Element Analysis,	None	Reliable assessment and prediction of slope performance and stability require modelling the linked T.H.M. processes in the slope.
Igwe and Chukwu [9]	Numerical method analysis via Geo Studio	None	The following factors have been identified: insufficient shear strength, rainfall, steep slopes, curvature, clay content, and water content. The most important factors that may compromise slope stability.
Gupta et al. [20]	Using numerical modelling, a critical assessment of the stability analysis of discard dump slopes was produced.	None	In addition to the factor of safety, significant output parameters are also outlined.
Gawain et al. [4]	FEM	No	Heat and mass transfer in saturated porous materials are fully coupled transient phenomena.
	A study was conducted on 2-Dimension limit equilibrium back-analyses.	In order to create stable bench configurations and a final slope, it was considered necessary to reduce the bench height and perform dewatering.	Mine slope movements occur near weak discontinuities due to several factors: the adverse positions of foliation planes and joints, along with low shear strength and significant rainfall that fills tension cracks.

It is rarely recognised how temperature directly influences the mechanical properties of non-freezing soils and how variations in vegetation cover, wind patterns, solar radiation, and air temperature may cause them to fluctuate [5]. Currently, the interdependent H-M or thermo-mechanical (T-M) effects are the primary focus of slope stability assessment studies. Not much research has been done on slope stability when considering coupled THM) effects, particularly when developing numerical models for these assessments. Incorporating thermal effects is crucial in these analyses, as slope instability and failure frequently result from temperature fluctuations during excavation and maintenance activities. As a result, this work, which examined the creation of evaluation markers for slope stability in connection with coupled THM processes, is vital [2].

In-depth research has been done to assess how coupled THM phenomena affect mine waste dump stability and, if required, to lessen the risk of slope failure during heavy rains and other harsh weather conditions.

Table 1 depicts that the evaluation and prevention of slope stability use numerical methods across different rainfall scenarios and soil types. Schmertmann [16] highlights the influence of slope angle, rainfall, and soil permeability on stability. The work of Zhao et al. [17] and Song [18] demonstrates that rainfall leads to soil infiltration, which lowers safety factors, and Masoudian et al. [19] show that persistent rainfall increases failure risk. The research of Wu et al. [2] supports THM model development, which includes interaction between multiple processes, and Igwe and Chukwu [9] emphasize how shear strength and clay content affect this interaction. The research by Gupta et al. [20] alongside Gawin et al. [4] demonstrates methods for slope design optimization and the prevention of failures near weak discontinuities.

Many critical observations can be made, including the following: It should be noted that a numerical methodology was used in the investigation. The quick development of computer science makes it clear. The most significant benefit of numerical modelling is its ability to accurately depict, using input data, the interplay between the structures under analysis and other influencing factors. Empirical or analytical research cannot accomplish this. Numerical computation results are diverse and particularly helpful when combined with the results of evaluations and testing in the laboratory. Despite the fact that excessive rainfall has been shown to have a significant impact on the stability of landslide prevention and mine waste dump slopes, measures have generally not been assessed or implemented [21].

Figure 1. IZUMA dump slope

Figure 2. Subsurface flow channels contribute to the erosion of slope material, compromise the stability of slope margins, and can ultimately lead to slope failures

Maamba Collieries Limited (MCL) has been involved in surface mining since 1967, initially relying on imports from the Wankie mine in Zimbabwe. After the UDA in 1965, the Nkandabwe mine was established, but operations ceased due to geological faults and flooding. MCL began mining in the Kanzinze basin, but production was temporarily moved to the Izuma basin in 1985. The dragline was repaired, and all coal mining operations were relocated to the Izuma basin to sustain production [22]. The Izuma dump slope has a long history of slope failures, primarily caused by the entry of surface water, which increases pore water pressure during heavy rainfall events. The slope's geology, characterised by weak bedding planes and fractures, worsens these problems, decreasing the slope material's shear strength. Therefore, our study will primarily concentrate on the Izuma dump slope.

Figure 1 shows that the mine slope presents well-defined trenching that both increases slope stability and minimizes potential failures. The slope structure features planned excavation strategies that produce gentle progressive layers among the inclines. The design approach functions well to minimize runoff while decreasing erosion levels and avoiding significant collapses, yet consistent observation of rainfall effects combined with adequate drainage systems is needed. Figure 2 highlights areas of instability, marked by blue boxes, indicating possible tension cracks or localized slope failures. Geological conditions coupled with steep terrain along with inadequate water drainage lead to these areas becoming compromised. Ongoing bench failures demonstrate the necessity for enhancing design approaches and drainage technologies and structural enhancements that promote enduring slope stability.

This study's objective is to calculate the stability of (IZUMA) the Maamba mine waste dump slope while accounting for combined THM factors. A quantitative analysis of slope stability was carried out, taking into consideration the potential effects of coupled THM phenomena on slope stability in order to protect the infrastructure, mining equipment, and local population along the Maamba mining waste dump slope.

The waste dump from the Maamba mine slope stability was evaluated numerically using COMSOL's finite difference method. This study also employed Geographic Information Systems (GIS) technology to acquire high-resolution photos of the Maamba coal mine waste dumps, yielding detailed spatial data essential for analysing slope stability under coupled THM factors. The GIS software facilitated the integration of multiple data layers, such as satellite imagery, topographic maps, and land use classifications, which were crucial for comprehending the geographical distribution and attributes of the waste dumps and their vulnerability to failure. The assessment accounted for the specific geo-mining characteristics of the waste dump, varied rainfall scenarios, and temperature and evaluated geotechnical features. The anticipated result will serve as a reference point for other instances of mine waste disposal in Zambia and the southern region of Africa.

2 Methodology

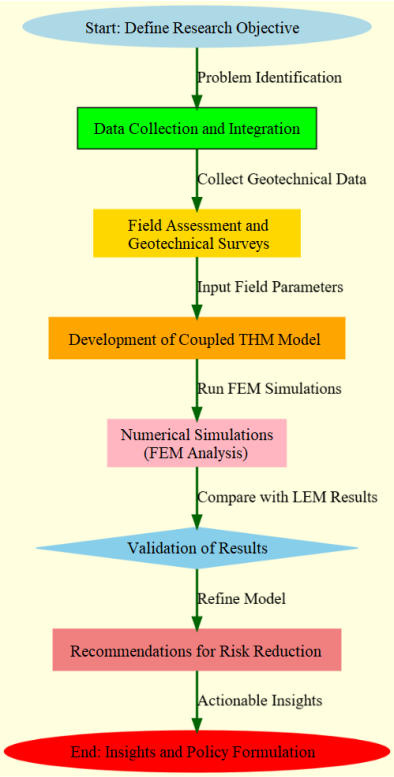

Figure 3. Proposed methodology diagram

Figure 3 presents a flowchart showing the structured process for evaluating slope stability and creating policy recommendations. Research initiatives begin with setting the objective, followed by problem identification and geotechnical data integration. Field observations and surveys deliver key data required for working with a system that unifies THM modelling. Numerical simulations employing FEM conduct slope stability analyses which LEM verifies through validation analysis. Flawless model development culminates in risk reduction recommendations, which create implementable strategies and policy initiatives for landslide risk mitigation.

2.1 Case Study

MCL is situated in the southern Zambian province of Mamba town, Sinazongwe district, in the Gwembe Valley, which is part of the Gwembe Coal Formation. It is roughly 350 kilometres from the capital, Lusaka, and is bordered by $17°22'0''$ South and $27°9'0''$ East.

The mine waste dump area is separated into two sections: the long-standing Izuma-A Dump and the recently opened Azuma-B Dump. In this study, we will focus on the Izuma-B Dump. An excess of 6.4 million cubic meters of overburden and waste material have been deposited in waste dumps at MCL. Kanzinze waste dumps constitute 63% of the overall volume, with the remainder originating from the Izuma dump. Since the commencement of mining operations, data indicate that more than 4 million m^3 of waste material has been deposited in the region. Presently, 20% of the output from the Drew Boy washer and the cyclones at the coal preparation plant is disposed of as waste material in the Kanzinze landfills. Annually, the coal preparation facility discharges an average of 110,000 tonnes of waste from the Drew Boy washer and 40,000 tons from the cyclones [22]. The overall inclines of the Maamba mine waste dump are modest, not surpassing 43°.

MCL is situated in the Lower Karoo System's Gwembe Coal Formation. There are three distinct units in the Gwembe Coal Formation: lower, middle, and upper [23]. The base unit is sandstone, while the intermediate and top units are claystone and coal. The central section consists of the primary coal deposit, which is situated above the carbonaceous and coal-rich mudstone layer. The primary coal layer has significant thickness variation and can transition horizontally into muddy sediment containing coal. Strata of sandstone and siltstone partition specific regions. The superimposed rocks display a dark hue, varying from grey to black. They are homogeneous and robust, consisting of silty mudstones or fine-grained siltstone. The thickness of the principal coal seam ranges from several millimetres to a maximum of 11 meters. The coal seams situated above the central seam often possess a thickness of about a few millimetres and seldom surpass 1.5 meters.

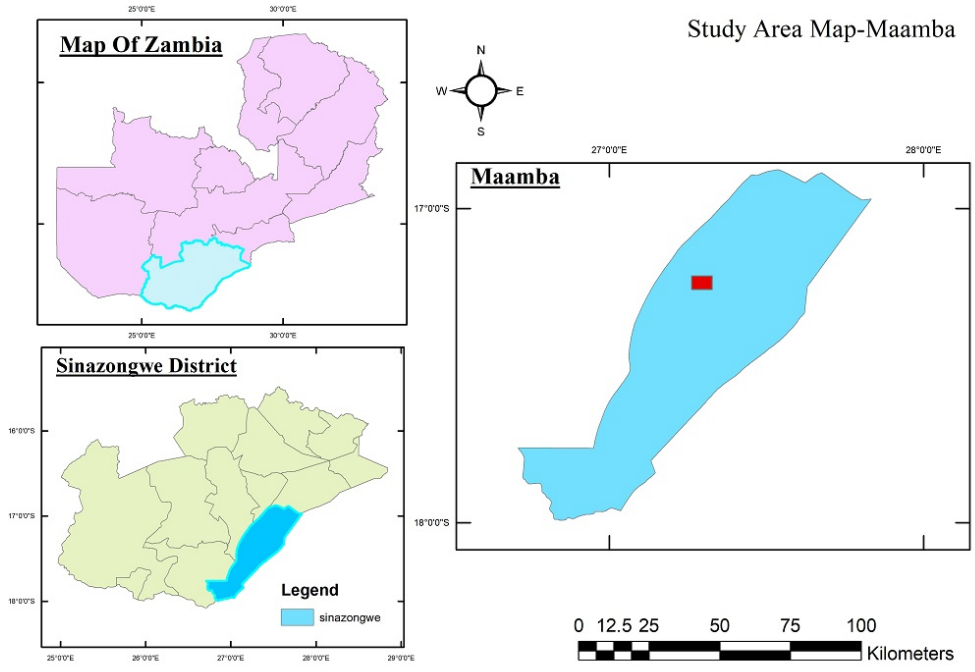

Figure 4. Study area map-Maamba

Incorporating Figure 4 and Figure 5 into the methodology section will significantly enhance the clarity of the paper by providing visual context for the study area and the geological challenges associated with it. Figure 4 presents a map illustrating the study area, including Zambia, Sinazongwe District, and Maamba, offering a clear geographical perspective and highlighting the specific focus of the research. Figure 5, the geologic map, depicts

the spatial distribution of rock types, formations, and faults, emphasizing the critical role of geological conditions in slope stability. These visual elements will aid readers in better understanding the study's context and the factors influencing slope stability in the region.

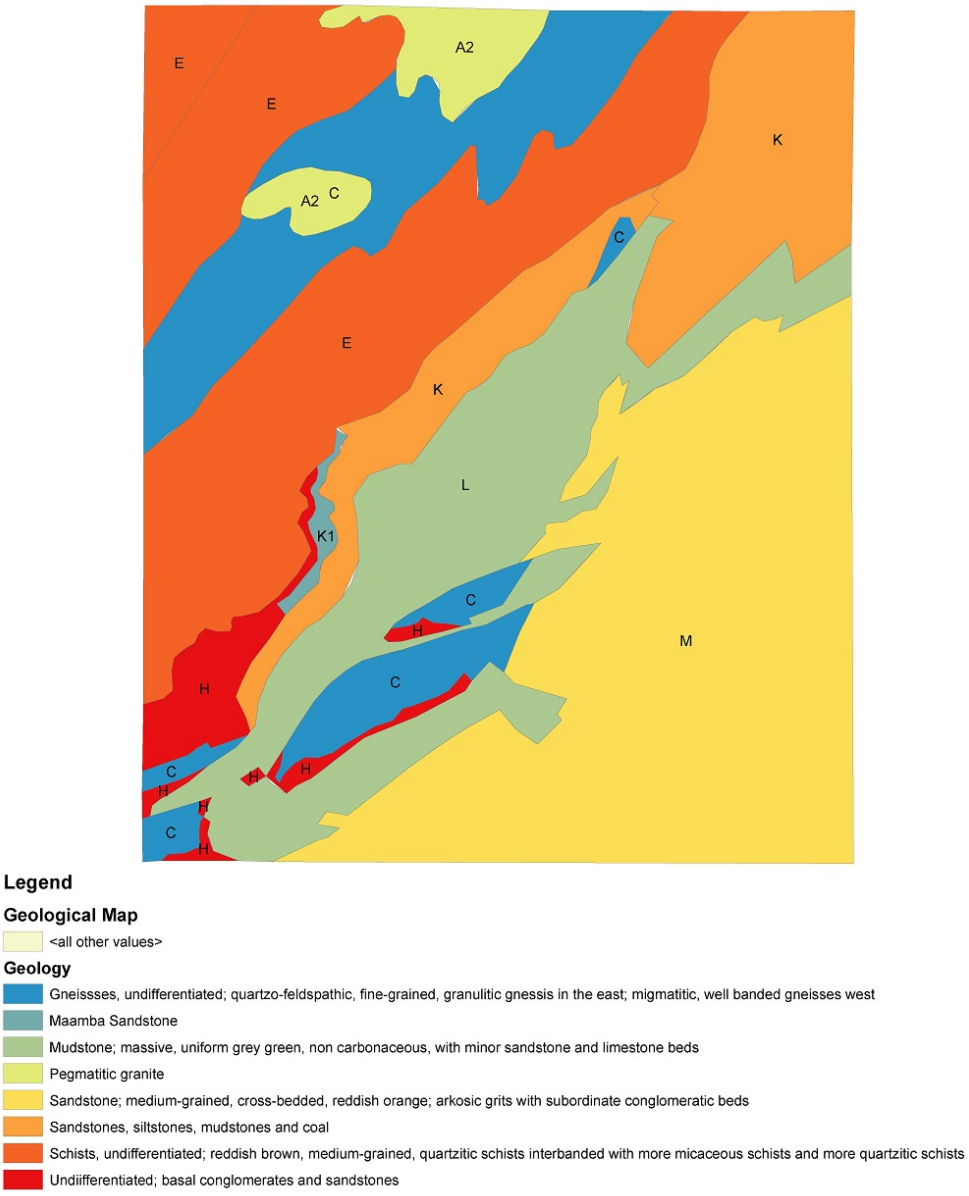

Figure 5. The study area's geological map

These figures comprehend the research problem more efficiently since they show the complex relationship between geology, hydrology and thermal conditions in the region. In addition to increasing the informative nature of the section, the incorporation of these visuals provides a better association between the methods mentioned and the actual problems being solved. This way, the inclusion helps achieve a closer connection between theory and practice and improves the study.

Figure 6 shows a geological succession starting from the Precambrian up to the present age with details about rock formations and lithologies and HCS parameter listings and measurements. The Kalahari Sands occupy the top position of the sequence with 50 m of thickness and the sequence continues downward with Jurassic Batoka Basalt and Upper Karoo sedimentary deposits of mudstone and sandstone that comprise significant reservoirs and seals. The Escarpment Grit and Madumabisa Mudstone serve as critical components of hydrocarbon systems. The Lower Karoo comprises coal-bearing sandstone and shale formations that contain oil and gas occurrences, with the Maamba Sandstone Member serving as an oil-producing formation. The sedimentary arrangement reveals strong indications that the area contains valuable hydrocarbon resources.

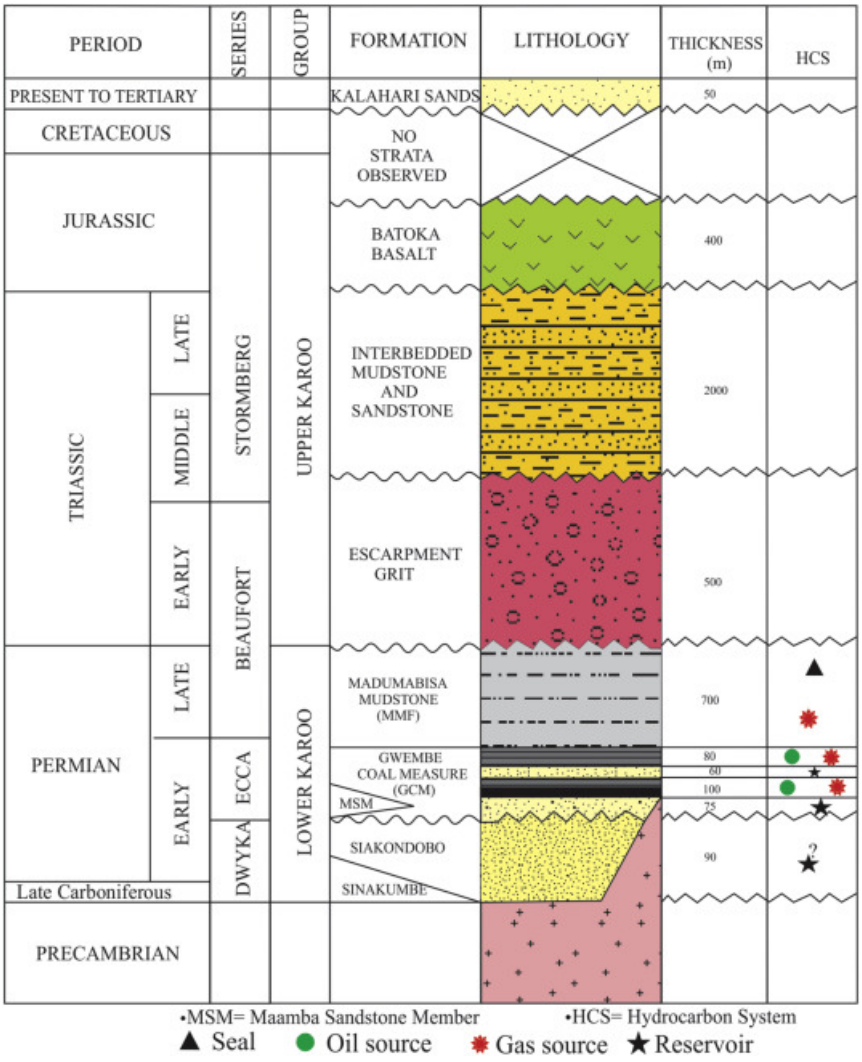

Figure 6. Moyes and Co.'s (2012) stratigraphic depiction of the Mid-Zambezi Valley basin; (http://www.moyesco.com)

The coal seams above the primary seam typically have a thickness of only a few millimetres and seldom exceed 1.5 meters [22].

The Mid-Zambezi Valley's Siankodobbo Coalfield contains the Maamba Coal Project area. Pegmatites intersect a series of metamorphic schists and gneisses that make up the mine area's basement. Three separate Karoo-aged lithostratigraphic units that cover the basement are visible within the MCL Permit limit. In the Siankodobbo Sandstone, the three successively arranged formations are the Madumabisa Mudstone Formation, Gwembe Coal Formation, and Gwembe Coal Formation. In areas without faulting, the dip of these strata typically varies between 1 and 5 degrees southerly.

2.1.1 Siankodobbo Sandstone Formation

The Siankodobbo Sandstone Formation can be split into three lithofacies assemblages, as described by the study [24]. These assemblages consist of diamictite, including both simple and complex forms, as well as layers of siltstone and sandstone. Additionally, they contain a type of large sandstone with fine to medium grain size. The assembly reaches a maximum thickness of 20 meters, with individual components stacked on each other, ranging in thickness from 1 to 90 centimetres. The siltstone assemblage indicates that it was formed by settling suspended particles, most likely at the bottom of a glacial lake. It also includes deposits formed by the flow of water beneath the surface, distinguished by cross-laminated sandstone and siltstone.

The non-carbonaceous sandstones with fine grains that make up the Siankodobbo Sandstone Formation are suddenly covered by the Gwembe Coal Formation. The only coal-bearing succession in Zambia's Zambezi Valley that is a member of the Karoo Supergroup is the Gwembe Coal Formation, which is identified by its highly carbonaceous, coarse-grained sandstones. The Gwembe Coal Formation reaches its maximum thickness of 280

meters in the centre of the Zambezi Valley.

The Gwembe coal formation is the result of river action depositing mudstones, siltstones, and sandstones in floodplains and channels. The formation's fourteen lithotypes are categorised into four facies associations: Sandstone A, Coal, Maamba Sandstone, and Murdock. The coal facies connection is composed of inner seam sandstone and coal lithofacies. The swampy, shallow portions of the floodplain form the Main Seam, also known as the lucrative coal seams, which range in thickness from 5 to 12 meters.

Characteristics of Sandstone The river flow pattern has shifted from a nearby braided system to a meandering stream system with pronounced sinuosity, according to a facies association. Due to discontinuity issues, the Minor Seams are excluded from the ore reserve calculation for the Izuma-A block, with the exception of the Major Coal Seam A&B, which is identified as Seam 1 to 5. Across the Izuma-A blocks, these primarily depositional formations show up as sizable pockets or lenses. They are frequently found between 10 and 50 meters below the topsoil and can range in thickness from 0.5 to 3 meters. It was discovered that these occurrences varied in thickness and frequency. Along the strata/beds, these seams typically show regular variations in both latitude and longitude. With a high sulfur content and notable ash percentages, the seams mostly have a glossy appearance [25].

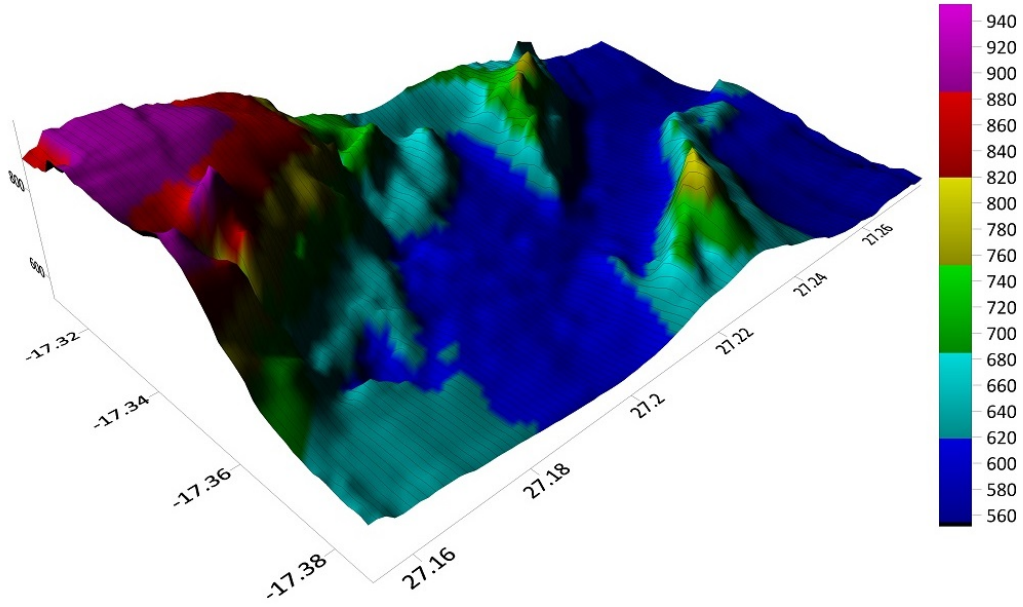

(a)

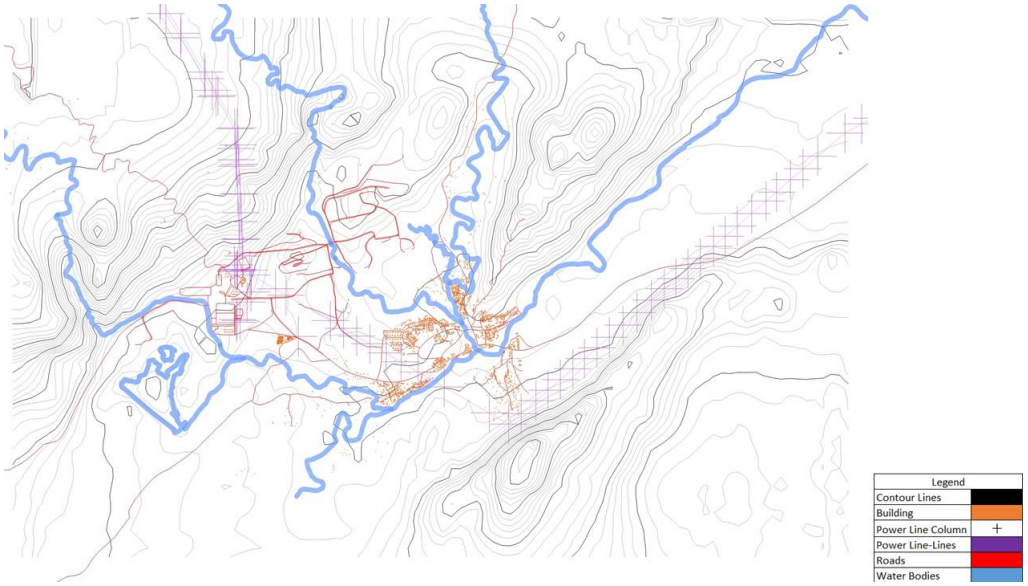

(b)

Figure 7. (a) General terrain 3D map of the study area, (b) General topography map of area study

2.1.2 The mudstone formation of Madumabisa

The late Permian Madumabisa Mudstone Formation covers the Gwembe Coal Formation. The maximum thickness is 700 meters, with four lithofacies that can be classified into two facies assemblages. These sediments are collectively of lacustrine origin.

Subgraph (a) of Figure 7 depicts the 3D topographic model that visualises the elevation distribution of a region, with elevation values ranging from 560 to 940 meters (color-coded). Peaks and valleys are evident, indicating areas with high relief and significant variations in terrain. This information is crucial for understanding slope stability, hydrological flow patterns, and potential areas of geological interest or risk, such as landslides.

Subgraph (b) of Figure 7 depicts the topographic map incorporating contour lines, water bodies, infrastructure (roads, buildings, power lines), and their spatial relationships. The blue water bodies and streams highlight drainage patterns, while contour lines depict elevation changes. This map aids in urban planning, risk assessment, and hydrological studies by integrating natural and built environments.

2.2 Geotechnical Waste's Characteristics Material at the Location Under Investigation

The majority of the material comprises mine waste elements such as claystone, mudstone, shale, sandstone, coal, and sandy formations, together with a mixture of clay, humus, and gravel.

Table 2. Properties of waste dump materials obtained via laboratory analyses

Parameters	Tested Result
Soil unit weight (kN/m^3)	19.613272
Friction angle (degree)	20
Cohesion (Pa)	25000
Bulk modulus (GPa)	0.32
Shear (GPa)	3.1

The experimental soil data provides fundamental mechanical information needed to evaluate slope stability alongside load-dependent soil behavioural dynamics (Table 2). Measurement of unit weight showed 19.613 kN/m^3, indicating the soil density relative to weight. The soil resists sliding through internal friction at 20° and displays inherent shear strength at 25,000 Pa against external pressure. The determination of bulk modulus at 0.32 GPa shows the degree of soil compression when subjected to uniform stress along with a shear modulus range of 3.1 GPa, demonstrating the resistance to shear deformation. Geotechnical analyses rely on these parameters for their foundation and stability assessment work.

2.2.1 Rainfall in the area of the Maamba mine waste dump

To show variation within the months and not just the monthly totals, Figure 8 shows the rainfall accumulated over a sliding 31-day period centred around each day of the year. Maamba experiences extreme seasonal variation in monthly rainfall. The month with the least rain in Maamba is July, with an average rainfall of 0.0 inches.

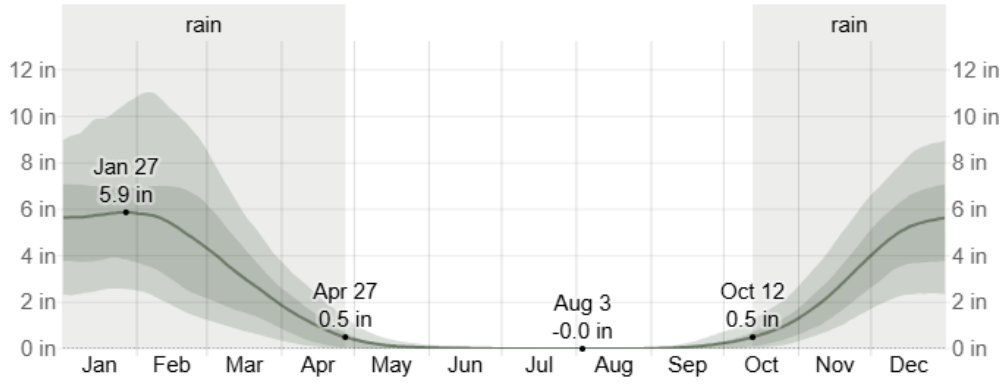

Figure 8. Maamba mine region rainfall data
Source: Spark, 2024

The Southern Province is predominantly located at an altitude ranging from 1100m to 1200m above mean sea level (AMSL). The project site is situated in an area with heights ranging from 575 to 689 meters above sea level (ASL). The area commonly encounters exceedingly high temperatures, especially in the arid season, which extends

from October to December. The maximum temperature recorded at MCL in November 2023 was 33.4°C, and the minimum was 22.7°C in July 2023. Typically, when rainfall is predictable, it appears in two forms: frequent heavy downpours of short duration and intermittent light rain of lengthy duration [26].

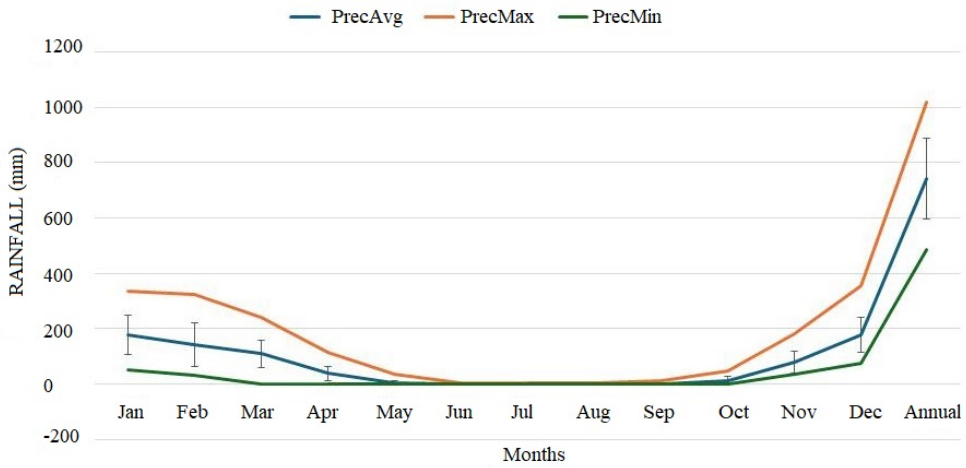

Figure 9. The 2023 annual rainfall data by month of study region

The annual average precipitation of 742.7 mm in the Maamba region suggests moderate rainfall. The most significant average monthly precipitation was 178.3 mm, recorded in January 2023. The highest amount of rainfall ever recorded in a year is 1020 (Figure 9).

The 145.1 mm standard deviation of yearly precipitation represents the inter-annual uncertainty in total rainfall, an essential factor for evaluating the dependability of water resources and preparing for possible slope instability. Significantly, February exhibits the most significant monthly standard deviation of 78.6 mm. This variability might be ascribed to the impact of climate change [27].

2.3 Theoretical Equations for the Coupled THM Model

The following is an expression of the effective stress in an unsaturated and deformable porous material, like a slope [28, 29]:

$$\sigma_{ij} = \sigma_e + \alpha\delta_{ij}p \tag{1}$$

where, σ_{ij} is the total stress vector, σ_e is the effective stress, α is Biot's coefficient, δ_{ij} is Kronecker's delta ($\delta_{ij} = 1; \delta_{i\neq j} = 0$), and p is the water and air mixture's average pressure.

$$p = S_w p_w + S_a p_a \tag{2}$$

S_w and S_a represent the air and water saturation levels in the porous media, respectively, and p_w and p_a are the pore water and air pressure.

2.4 Constitutive Relationship Between Thermo Elasticity, Plasticity, and Thermal Resistance

The following is an expression for the thermo-elastic-plastic constitutive equations [2]:

$$\sigma_e = \mathrm{D}\varepsilon_e = \mathrm{D}\left(\varepsilon - \varepsilon_p - \varepsilon_t\right) \tag{3}$$

where, D is the elasticity matrix, and $\varepsilon, \varepsilon_e, \varepsilon_p$, and ε_t are the total strain, elastic strain, plastic strain, and thermal strain, respectively. The elasticity matrix D can be articulated in terms of Lamé parameters. λ and μ in the following form:

$$D = \begin{bmatrix} \lambda+2\mu & \lambda & \lambda & 0 & 0 & 0 \\ \lambda & \lambda+2\mu & \lambda & 0 & 0 & 0 \\ \lambda & \lambda & \lambda+2\mu & 0 & 0 & 0 \\ 0 & 0 & 0 & \mu & 0 & 0 \\ 0 & 0 & 0 & 0 & \mu & 0 \\ 0 & 0 & 0 & 0 & 0 & \mu \end{bmatrix} \tag{4}$$

where, λ and μ can be determined, respectively, by the following equations:

$$\lambda = \frac{Ev}{(1+v)(1-2v)} \tag{5}$$

$$\mu = \frac{E}{2(1+v)} \tag{6}$$

where, E is the elastic modulus and v is the Poisson's ratio.

The following equation can obtain the thermal strain in the porous medium:

$$d\varepsilon_t = \beta_t \delta_{ij} dT \tag{7}$$

where, β_t is the coefficient of linear thermal expansion, and T is the porous media's solid matrix temperature.

2.4.1 Geometric deformation equation

For minor deformations, the geometric equation of deformation is written as follows:

$$\varepsilon_{ij} = \frac{1}{2}\left(u_{i,j} + u_{j,i}\right) \tag{8}$$

where, u is the displacement within the framework of the porous medium.

2.4.2 Equation representing mechanical equilibrium

Based on the idea of momentum balance and disregarding the effects of inertia, the subsequent statement can be derived for mechanical equilibrium:

$$\Delta\sigma_{ij} + \rho_{\mathrm{eq}} g_i = 0 \tag{9}$$

Title numbers have been added, and the numbering sequence has been checked for consistency throughout the manuscript.

where, g_i represents the gravity vector and ρ_{eq} represents equivalent bulk density.

$$\rho_{eq} = (1-n)\rho_s + nS_w\rho_w + S_a\rho_a \tag{10}$$

where, ρ_s, ρ_w and ρ_a are the densities of the solid matrix, liquid water, and dry air, respectively, and n is the porosity of the porous medium. The densities of liquid water and dry air are influenced by temperature [30].

$$\rho_w = 314.4 + 685.6\left\{1 - \left[\left(T_w - 273.15\right)/374.14\right]^{1/0.55}\right\}^{0.55} \tag{11}$$

$$\rho_a = \frac{M_a}{R_a T_a} p_a \tag{12}$$

where, M_a is the molar mass of air, T_w and T_a are the temperatures of water and air, respectively, and R_a is the universal gas constant for air.

2.4.3 COMSOL based on Richard's equation

The flow of water in both unsaturated and saturated states within a porous medium is described by the modified Richards' Equation, which does not take into consideration the compressibility of solid particles and liquid water [31].

$$C \cdot \frac{\partial H_p}{\partial t} + \nabla \cdot \left[-K\nabla\left(H_p + Z\right)\right] = Q_m \tag{13}$$

where, Hp is the pressure head, t is the time, K is the hydraulic conductivity, Z is the vertical elevation coordinate, Qm is the water seepage source, and C is the volumetric specific humidity.

2.4.4 COMSOL-based van Genuchten equations

The van Genuchten equations provide a description of the variations in C and K [32]:

$$C = \begin{cases} \frac{\alpha m}{1-m}\left(\theta_s - \theta_r\right) S_e^{\frac{1}{m}} \left(1 - S_e^{\frac{1}{m}}\right)^m & H_p < 0 \\ 0 & H_p \geq 0 \end{cases} \tag{14}$$

$$K = \begin{cases} {S_e}^l \left[1 - \left(1 - S_e^{\frac{1}{m}}\right)^m\right]^2 & H_p < 0 \\ 1 & H_p \geq 0 \end{cases} \tag{15}$$

where, m, and l are the porous medium's constants; θ_s and θ_r are respectively the residual water content and the saturated water content; S_e symbolizes the proper saturation, which is further expressed as:

$$S_e = \begin{cases} \frac{1}{[1+|\alpha H_p|^n]^m} & H_p < 0 \\ 1 & H_p \geq 0 \end{cases} \tag{16}$$

2.4.5 Thermal equations

Due to the low likelihood of heat convection in dry air, dry air heat transfer is not considered in this analysis. Moreover, the heat generated by the porous medium's deformation and the groundwater's viscous dissipation are not considered. Fourier's law can be used to write the following equation, which causes the water and the porous media to have a thermal energy balance [33]:

$$\begin{aligned} (1-n)\rho_s c_s \frac{\partial T}{\partial H_p} + nS_w\rho_w c_w \frac{\partial T_w}{\partial t} = \Delta\left[(1-n)\lambda_s \Delta T + nS_w\lambda_w \Delta T_w\right] \\ +S_w\rho_w c_w \Delta\left[T_w\left(K\Delta\left(H_p + Z\right)\right)\right] - (1-n)T\beta_t \frac{\partial\left(\delta_{ij}\varepsilon_{ij}\right)}{\partial t} \end{aligned} \tag{17}$$

where, c_s and c_w are the water's and the solid matrix's respective specific heat capacities and λ_s and λ_w are the water's and the solid matrix's respective thermal conductivities.

2.5 Model Simulation

The basic concepts of soil slope stability, including soil mechanical characteristics, thermal transfer mechanisms, and hydric migration processes, were first investigated in this study. The following presumptions were made prior to starting the mathematical construction of the coupled model THM [9]:

(1) The water, solid, and dry air are all taken into account as distinct entities in the slope, which is a continuous porous medium. Dry air is considered an ideal gas. Even though the structure of the porous medium may alter, the solid particles remain incompressible.

(2) Water is thought to have an isotropic elastoplastic structure, and its viscosity is thought to be temperature-independent despite the fact that its density varies with temperature.

3 Results

A segment from the waste area has been designated as Izuma waste B. The geometry is depicted in the drawings below. The dimensions are 93 meters horizontally and 42 meters vertically, consistent with the actual measurements on-site.

As shown in Figure 10, this paper features the schematic layout of the analysed soil slope in terms of dimensions, slope angles, and boundary conditions. The geometry of the structure requires the construction of a 93-meter-long horizontal part of the structure, a 42-meter vertical part of the structure, and an inclined plane with a slope of 39 degrees. The boundaries, heights, and plans of terrain on the slope and other structural elements are designated. This figure forms the basis from which the geometry discussed in the subsequent simulations is seen.

3.1 Model Simulation with FEM

The shear strength reduction methodology is widely used in the FEM analysis of slope stability. Dividing the actual strength data by a trial factor F_{trail} yields each set of shear strength parameters in the shear strength reduction FEM analysis of slope stability. Thus, the internal friction angle ϕ_{Trial} and the reduced cohesiveness c_{trial} can be expressed as [34].

$$c_{trial} = c/F_{trail} \tag{18}$$

$$\phi_{Trial} = \arctan\left(\tan\phi/F_{trial}\right) \tag{19}$$

where, c and ϕ stand for the cohesion and internal friction angles, respectively. The procedure for the aforementioned trial calculation continues when the slope reaches the critical limit state, and the factor of safety (FOS) corresponds to the critical trial factor and can be found as follows:

$$FOS = c/c' = \tan\varphi/\tan\varphi' \tag{20}$$

At the critical limit state, the internal friction angle is represented by ϕ' and the reduced cohesion by c'. This study establishes the critical limit state, also referred to as the criterion for deformation break, which is consistent with the FEM calculation's non-convergence results.

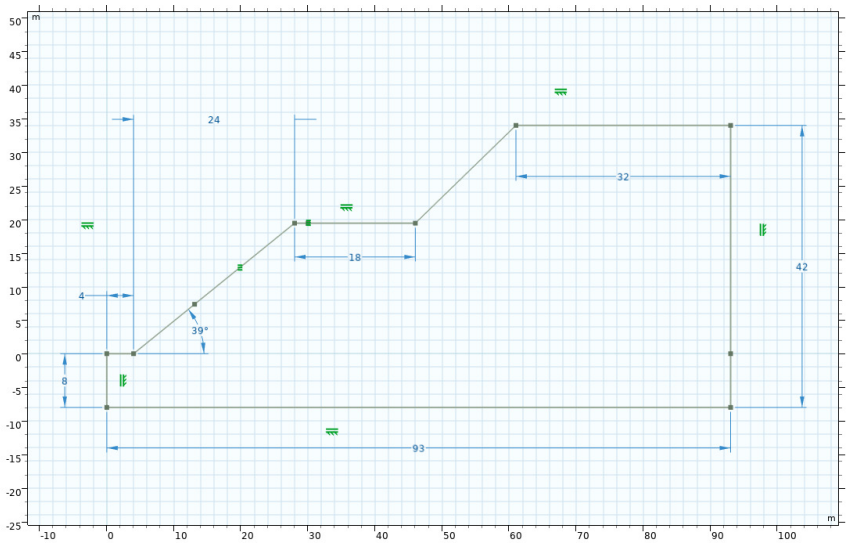

Figure 10. Schematic representation of the soil slope under investigation

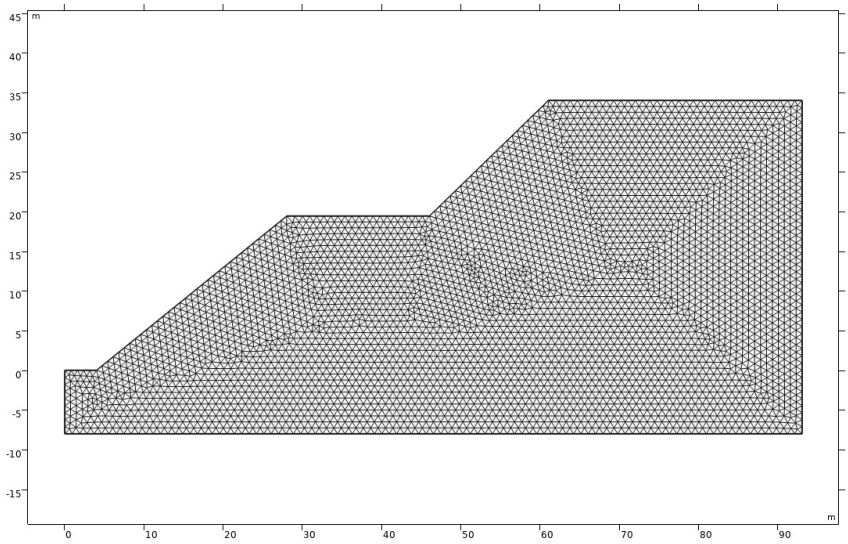

Figure 11. Mesh creation of the analysed slope geometry

Three methods for modelling slope stability prediction are identified in this section: coupled H-M analysis, coupled THM analysis, and mechanical (M) analysis. The models used for the simulation are shown in Figure 10. As shown in Figure 11, the soil slope geometry is then incorporated into COMSOL Multiphysics for mesh generation. Table 3 lists the input variables, boundaries, constraints, and initial settings for each scheme, along with the model simulations. This research aimed to develop models that accurately represent the circumstances of the on-site slopes to establish a solid basis for slope stability assessments. Our methodology entailed doing an extensive field survey of the Izuma dump slopes to acquire precise topographical data. The acquired data were subsequently incorporated into our numerical models, guaranteeing that the simulations accurately reflect actual site circumstances.

Table 3. The model simulations of each scheme are presented herein, together with the input variables, boundaries, constraints, and initial settings

	M	H-M	THM
Solid material parameters			
Young's modulus (Pa)	1e+8	1e+8	1e+8
Poisson's ratio	0.4	0.4	0.4
Density (kg/m^3)	2000	2000	2000
Cohesion (Pa)	25000	25000	25000
Internal friction angle (°)	30	30	30
Conductivity of heat [W/(m·K)]	inapplicable	inapplicable	1.16
Capacity for specific heat [J/(kg·K)]	inapplicable	inapplicable	840
Coefficient of thermal expansion (1/K)	inapplicable	inapplicable	5e-7
Hydraulic conductivity (m/s)	inapplicable	8.25log-5	8.25log-5
V.G. model parameters as in equation [8]-[12]			
θ_s	inapplicable	0.5	0.5
θ_r	inapplicable	0.05	0.05
α	inapplicable	14.5	14.5
m	inapplicable	2.68	2.68
L	inapplicable	0.5	0.5
Liquid material parameters			
Density (kg/m^3)	inapplicable	According to Eq. (11)	According to Eq. (11)
Reference density (kg/m^3)	inapplicable	1000	1000
Conductivity of heat [W/(m·K)]	inapplicable	inapplicable	0.6
Coefficient of thermal expansion (1/K)	inapplicable	0.00002	0.00002
Mechanical module			
Slope top	unbounded	unbounded	unbounded
Slope surface	unbounded	unbounded	unbounded
Base of the slope	unbounded	unbounded	unbounded
Slope bottom	Rigid	Rigid	Rigid
Slope lateral sides	Roiler support	Roller support	Roller support
Force of volume	Gravitational Force	Gravitational Force	Gravitational Force
Hydraulic module			
Slope top	inapplicable	Mass flow rate (3×10^{-5} kg/m^2·s)	Mass flow rate (3×10^{-5} kg/m^2·s)
Slope surface	inapplicable	Open	Open
The base of the slope	inapplicable	Open	Open
Slope bottom	inapplicable	No continuity	No continuity
Slope lateral sides	inapplicable	No continuity	No continuity
Thermal module			
Slope top	inapplicable	inapplicable	35°C
Slope surface	inapplicable	inapplicable	35°C
The base of the slope	inapplicable	inapplicable	35°C
Slope bottom	inapplicable	inapplicable	15°C
Slope lateral sides	inapplicable	inapplicable	15°C
Initial temperature	inapplicable	inapplicable	15°C

3.1.1 Slope stability analysis considering mechanical effects

The internal angle of friction and cohesiveness of the soil is decreased using the finite element strength reduction method. Structural Mechanics module of COMSOL Multiphysics incorporates the model's mechanical equations for computations. Under the mechanical effect, the soil slope's FOS is 1.21 since F_{trial} is set to 1.21 when the computational results do not converge.

Figure 12 displays the distribution of the corresponding slope's plastic zone at this particular instant, t0. Additionally, when there is no convergence in the computation results, Figure 12 demonstrates that the most significant amount of plastic strain within the slope is 0.18. Furthermore, the illustration indicates that the critical limit condition is satisfied by the critical slip surface allocation within the slope.

3.1.2 Slope stability analysis considering $H - M$ effects

The Fluid Flow and Structural Mechanics modules of COMSOL implement mechanical and hydraulic equations for the derived model, respectively. These modules are responsible for implementing the model. The COMSOL software introduces a coupling between the two components. The values and input parameters utilised in coupled

Table 3 contain a list of computations. After loading the hydro effect for 0 to 60 minutes, The strength reduction method is used to evaluate the slope's stability state. F_{trial} equals 1.17 when the computation process does not converge. Consequently, the FOS of the slope is 1.17, which is 0.04 lower than the FOS of the slope in the presence of only the mechanical effect. This suggests that the slope FOS is reduced by nearly 4% due to the coupled H-M effect.

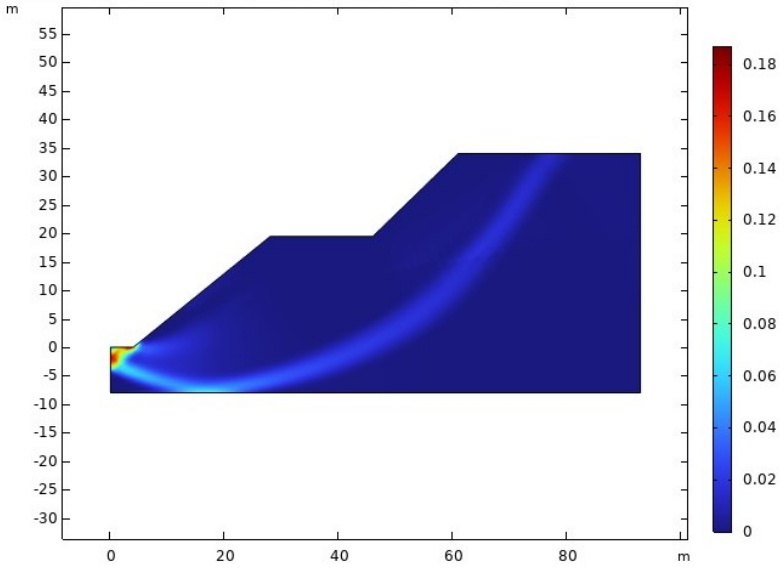

Figure 12. Plastic zone distribution under the M effect

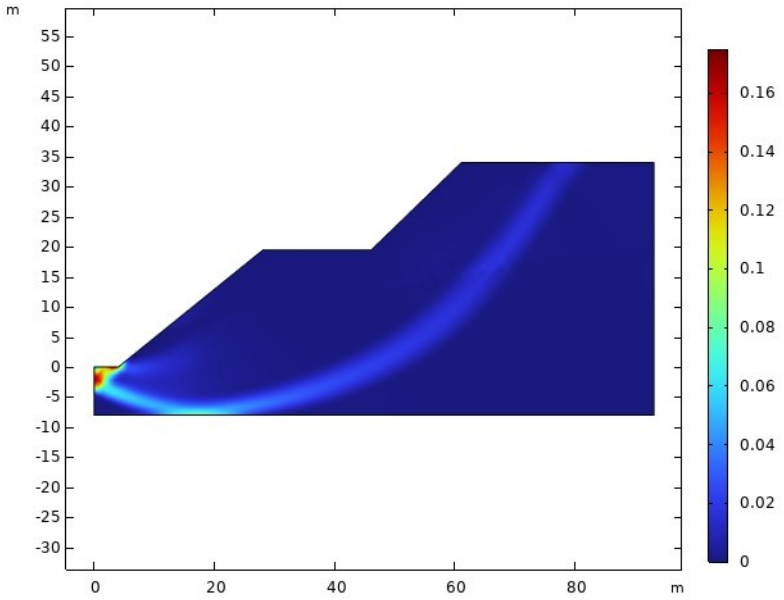

Figure 13. Plastic zone distribution under the H-M effect

The distribution of the plastic zone within the slope is shown in Figure 13. The figure shows, when the critically steady condition is reached, the slope's maximum plastic strain is 0.16, which is significantly less than the value under the effect of M (0.18). This suggests that the material properties of the slope were weakened by the effects of H-M couplings.

3.1.3 Slope stability analysis considering THM effects

The developed model's THM equations are implemented by the COMSOL Multiphysics "Heat Transfer," "Structural Mechanics," and "Fluid Flow" modules, respectively. COMSOL satisfies the requirement to couple all three sets of equations. After applying all T, H, and M loads from t0 for 60 minutes, the stability of the slope is examined using the strength reduction FEM. F_{trial} is determined to be 1.153 when the computation results show no

convergence. Thus, the FOS of the slope influenced by the coupled THM processes is 1.153, which is 0.32 less than that of the mechanical effect and 0.017 less than that of the coupled H-M effect. This indicates that, in comparison to using the M effect alone, the slope's FOS is decreased by more than 30% when both thermal and hydro processes are employed.

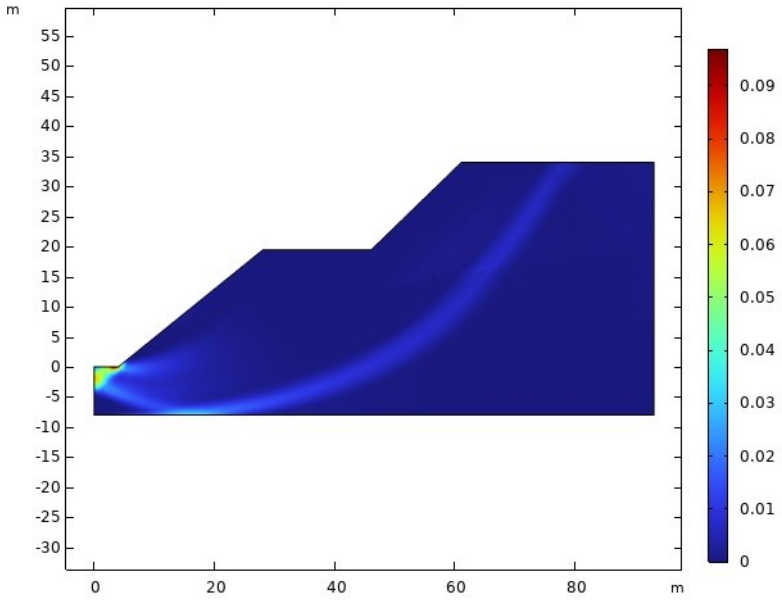

Figure 14. Distribution of plastic zone under THM effect

Figure 14 illustrates how the coupled THM processes affect the distribution of the plastic zone within the slope. At the critical steady state, the slope's maximum plastic strain is 0.09.

3.2 Analysis Utilizing the LEM

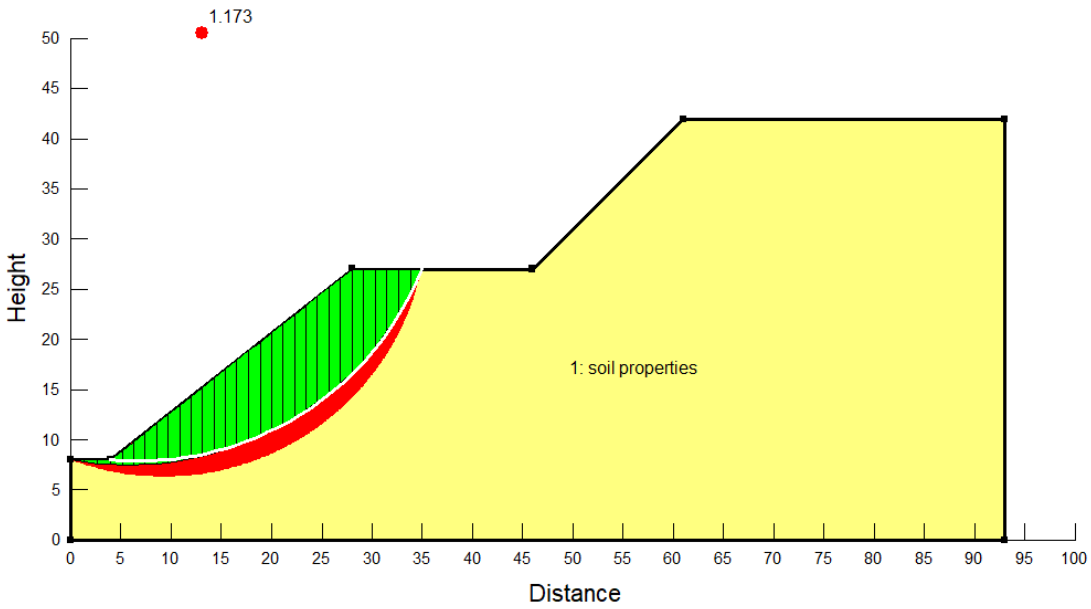

Figure 15. LEM analysis under M effect

A slope stability analysis is conducted using the traditional LEM in the Geo-Studio software. Slope stability analysis in our case study is made simpler by Geo-Studio's SLOPE (W), SEEP (W), and TEMP (W) modules. Although the SLOPE/W and SEEP/W modules are utilised for analysis under the coupled H-M effect, the SLOPE/W module enables limit equilibrium analysis of slope stability while accounting for the M effect. The limit equilibrium analysis of slope stability incorporating THM couplings is performed using the TEMP/W, SEEP/W, and SLOPE/W

modules. Table 3 displays the relevant input parameters and values used in the computation of limit equilibrium. The specific results of the limit equilibrium analysis for slope stability are shown in Figures 13, 14, and 15. The red area in the figure represents the total number of possible slip surfaces on the slope.

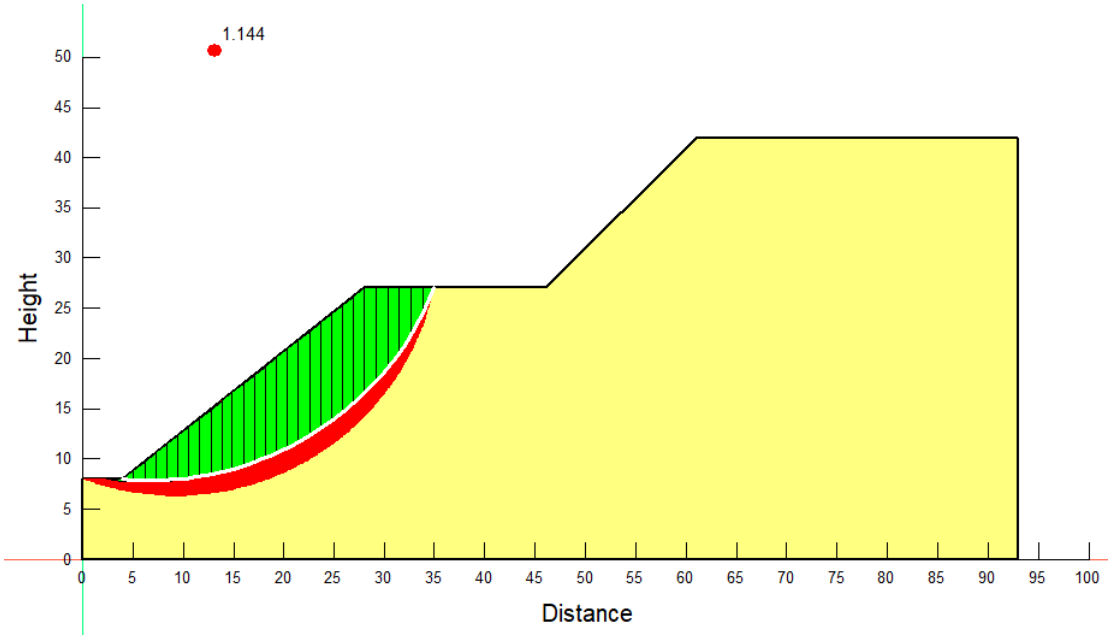

Figure 16. LEM analyses under H-M effect

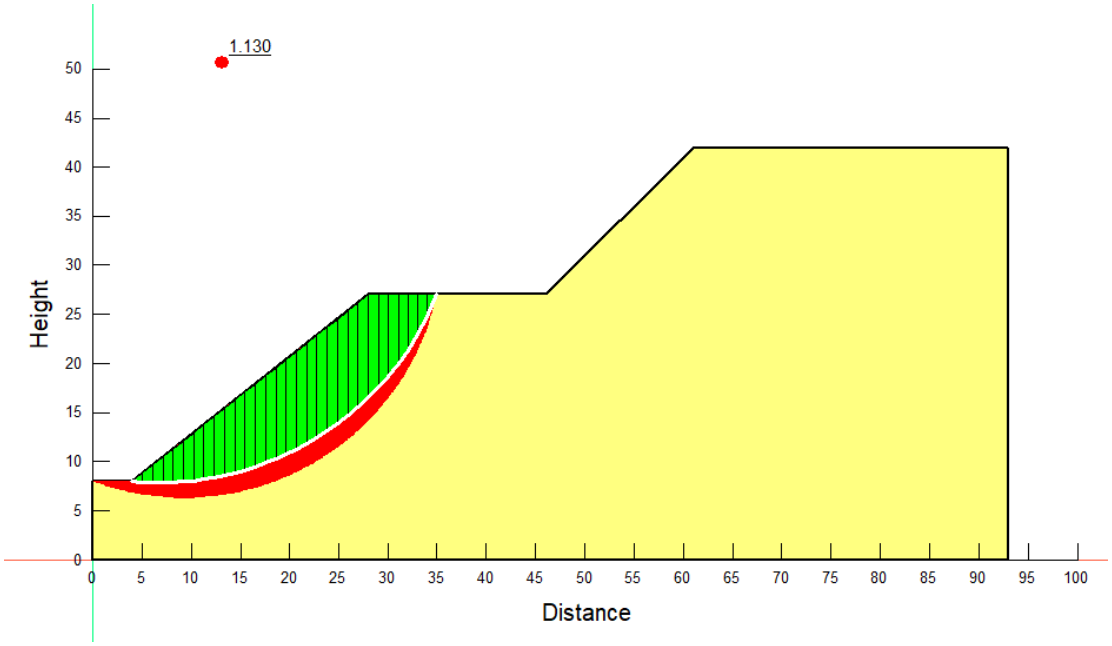

Figure 17. LEM analyses under THM effect

According to Figure 16 and Figure 17, the slope safety factors under the Mechanical, coupled H-M, and THM effects that were determined using the conventional LEM are 1.173, 1.144, and 1.130, respectively. The limit equilibrium calculation results demonstrate that adding thermal and hydro loadings to the mechanical process lowers the safety factor, which is consistent with the outcomes of the simulation model mentioned above.

Figure 18 shows the displacement profile of the slope. The deformation peaked at 400 mm and remained remarkably constant with little movement of the slope materials. The slope surface's displacement profile indicates the sliding surface's location at the slope's base.

The paper emphasizes the understanding of specific aspects of coupled THM behaviour in terms of slope stability and its relevance to safety factors. This work further supports the effects that these factors magnify slope instability: the safety factors reduce with M, H-M, and THM effects on the models. The implication is that when THM coupling is concerned, the safety factor of less than 1.4 obtained through conventional modelling is drastically reduced by over 30 percent. This important factor necessitates the adoption of methodologies that not only take into account these interrelated effects but also their significance.

These results can be useful in other mining-related areas with similar geophysical and hydro meteorological conditions, such as areas with sedimentary basins or high rainfall intensity. The study findings are a solid basis for calculating failure risks in similar situations and building preventive slope protection and anti-landslide systems. It also compares with conventional limit equilibrium approaches in lending a more practical outlook to the numerical methods.

The significance of this study goes far beyond the Izuma waste dump because the results can be used to develop a stability index for modelling slope stability under coupled actions. This analysis moves such field and modelling approaches forward to broaden applied and theoretical knowledge to enhance future decision-making of slope management and hazard reduction.

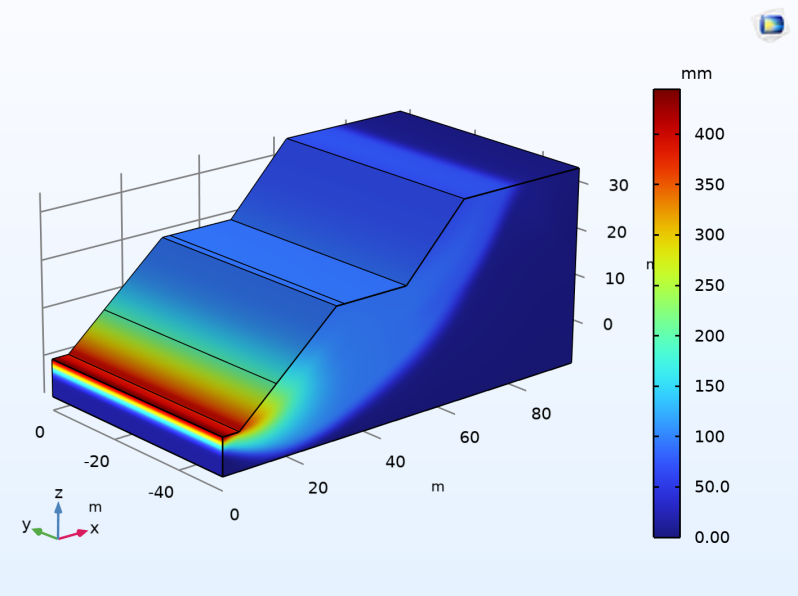

Figure 18. Displacement profile in millimeters along the surface of the geometry

4 Discussion

The Table 4 displays the FOS comparison between the results of the limit equilibrium calculations and the model simulation.

Table 4. Depicts FEM and LEM simulation results collectively with their deviations

	M Effect H-M Coupling	THM Coupling
Model simulation	1.21	1.153
	1.17	
Limit equilibrium results	1.173	1.13
	1.144	
Deviation	3.7%	2.3%
	2.6%	

According to Table 4, the FEM yielded results for the three schemes that were 3.7%, 2.6%, and 2.3% higher than those determined by the conventional LEM. The acceptable differences between the two methods indicate that the simulation results of the model agree well with the results of the LEM. Consequently, the validity of the developed model has been confirmed.

This study's outcomes align with the findings of the study [2], which demonstrated that precise assessment and prediction of slope performance and stability require modelling encompassing THM processes in unsaturated slopes.

The data presented in Figure 4 demonstrates a comparable pattern, indicating that the correlated THM processes affect the slope's FOS. This agreement validates the trustworthiness of our experimental methods and strengthens the applicability and generalizability of the study conclusions about slope stability [2].

It is important to note that while the general trends found in our analysis are consistent with the results of the study [13], notable differences could be attributed to modifications in the geotechnical characteristics of the material or soil that was examined in the models. The complexity of THM coupling mechanisms in slopes and other geotechnical contexts is highlighted by these discrepancies, underscoring the need for additional research in this area.

5 Conclusions

The results of the case study allow for the following deductions. A coupled THM model has been developed to assess slope stability, and the outcomes of its predictions have been contrasted with information from traditional limit equilibrium calculations. The model's applicability for evaluating slope stability even in real-world site conditions was validated by the strong correlation that was found between the two outcome sets.

In reference to numerical simulations of slope behaviour under the THM coupled process, the modelling outcomes aligned with the data from the referenced case study. Analysing slope stability under THM couplings is made easier by the developed model for slopes, which has been confirmed to generate precise and comprehensive predictions for evaluating slope performance, even in the context of mine dump slopes. Insightful data for planning slope reinforcement and evaluating remediation and landslip prevention techniques can also be obtained from the proposed model.

6 Future Scope

The slope was taken to be uniform for this investigation. To assess slope stability, a coupled THM model has been created, and the expected outcomes have been contrasted with data from standard limit equilibrium calculations. The two outcome sets showed a strong correlation, suggesting that the model is feasible for evaluating slope stability even in real-world site conditions.

Prospective projects will concentrate on enhancing the model to integrate more intricate and realistic characteristics, like the slope's variability. The study will examine the impact of various layers and strata on the overall stability of the slope.

Data Availability

The data used to support the findings of this study are available from the corresponding author upon request.

Conflicts of Interest

The authors declare that they have no conflicts of interest.

References

[1] H. Basahel and H. Mitri, "Application of rock mass classification systems to rock slope stability assessment: A case study," *J. Rock Mech. Geotech. Eng.*, vol. 9, no. 6, pp. 993–1009, 2017. https://doi.org/10.1016/j.jrmge.2017.07.007

[2] D. Wu, T. Deng, W. Duan, and W. Zhang, "A coupled thermal-hydraulic-mechanical application for assessment of slope stability," *Soils Found.*, vol. 59, no. 6, pp. 2220–2237, 2019. https://doi.org/10.1016/j.sandf.2019.12.007

[3] A. Rahimi, H. Rahardjo, and E. C. Leong, "Effect of antecedent rainfall patterns on rainfall-induced slope failure," *J. Geotech. Geoenviron. Eng.*, vol. 137, no. 5, pp. 483–491, 2011. https://doi.org/10.1061/(ASCE)GT.1943-5606.0000451

[4] D. Gawin, B. A. Schrefler, and M. Galindo, "Thermo-hydro-mechanical analysis of partially saturated porous materials," *Eng. Comput.*, vol. 13, no. 7, pp. 113–143, 1996. https://doi.org/10.1108/02644409610151584

[5] R. Oorthuis, J. Vaunat, M. H"urlimann, A. Lloret, J. Moya, C. Puig-Polo, and A. Fraccica, "Slope orientation and vegetation effects on soil thermo-hydraulic behavior. an experimental study," *Sustainability*, vol. 13, no. 1, p. 14, 2020. https://doi.org/10.3390/su13010014

[6] R. A. Shakesby and J. R. Whitlow, "Failure of a mine waste dump in zimbabwe: Causes and consequences," *Environ. Geol. Water Sci.*, vol. 18, no. 2, pp. 143–153, 1991. https://doi.org/10.1007/BF01704668

[7] H. J. Siddle, M. D. Wright, and J. N. Hutchinson, "Rapid failures of colliery spoil heaps in the south wales coalfield," *Q. J. Eng. Geol. Hydrogeol.*, vol. 29, no. 2, pp. 103–132, 1996. https://doi.org/10.1144/GSL.QJEGH.1996.029.P2.02

[8] D. Petley, "Global patterns of loss of life from landslides," *Geology*, vol. 40, no. 10, pp. 927–930, 2012. https://doi.org/10.1130/G33217.1

[9] O. Igwe and C. Chukwu, "Slope stability analysis of mine waste dumps at a mine site in southeastern Nigeria," *Bull. Eng. Geol. Environ.*, vol. 78, pp. 2503–2517, 2019. https://doi.org/10.1007/s10064-018-1304-8

[10] H. Rahardjo, A. S. Nio, E. C. Leong, and N. Y. Song, "Effects of groundwater table position and soil properties on stability of slope during rainfall," *J. Geotech. Geoenviron. Eng.*, vol. 136, no. 11, pp. 1555–1564, 2010. https://doi.org/10.1061/(ASCE)GT.1943-5606.0000385

[11] K. M. Neaupane, T. Yamabe, and R. Yoshinaka, "Simulation of a fully coupled thermo–hydro–mechanical system in freezing and thawing rock," *Int. J. Rock Mech. Min. Sci.*, vol. 36, no. 5, pp. 563–580, 1999. https://doi.org/10.1016/S0148-9062(99)00026-1

[12] B. François, L. Laloui, and C. Laurent, "Thermo-hydro-mechanical simulation of atlas in situ large scale test in boom clay," *Comput. Geotech.*, vol. 36, no. 4, pp. 626–640, 2009. https://doi.org/10.1016/j.compgeo.2008.09.004

[13] C. Zhou and C. W. W. Ng, "A thermomechanical model for saturated soil at small and large strains," *Can. Geotech. J.*, vol. 52, no. 8, pp. 1101–1110, 2015. https://doi.org/10.1139/cgj-2014-0229

[14] P. Kolapo, G. O. Oniyide, K. O. Said, A. I. Lawal, M. Onifade, and P. Munemo, "An overview of slope failure in mining operations," *Mining*, vol. 2, no. 2, pp. 350–384, 2022. https://doi.org/10.3390/mining2020019

[15] Z. Zhan, "Thermo-hydro-mechanical coupled material point method and its applications in landslide analysis," Dissertations, Hong Kong Polytechnic University, 2024.

[16] J. H. Schmertmann, "Estimating slope stability reduction due to rain infiltration mounding," *J. Geotech. Geoenviron. Eng.*, vol. 132, no. 9, pp. 1219–1228, 2006. https://doi.org/10.1061/(ASCE)1090-0241(2006)132:9(1219)

[17] X. T. Zhao, X. C. Gao, and D. S. Li, "The stability analysis of nantong coal mine waste dump, chongqing and prevention measures," *Appl. Mech. Mater.*, vol. 204, pp. 3526–3531, 2012. https://doi.org/10.4028/www.scientific.net/AMM.204-208.3526

[18] Y. S. Song, "Numerical analysis of the seepage from and stability of a mine waste-dump slope during rainfall," *J. Eng. Geol.*, vol. 25, no. 1, pp. 57–66, 2015. https://doi.org/10.9720/kseg.2015.1.57

[19] M. S. Masoudian, M. A. H. Afrapoli, A. Tasalloti, and A. M. Marshall, "A general framework for coupled hydro-mechanical modelling of rainfall-induced instability in unsaturated slopes with multivariate random fields," *Comput. Geotech.*, vol. 115, p. 103162, 2019. https://doi.org/10.1016/j.compgeo.2019.103162

[20] G. Gupta, S. K. Sharma, G. S. P. Singh, and N. Kishore, "Numerical modelling-based stability analysis of waste dump slope structures in open-pit mines-a review," *J. Inst. Eng. India Ser. D*, vol. 102, no. 2, pp. 589–601, 2021. https://doi.org/10.1007/s40033-021-00277-y

[21] P. Nguyen, A. Wrana, S. Rajwa, Z. R'o.za'nski, and R. Frączek, "Slope stability numerical analysis and landslide prevention of coal mine waste dump under the impact of rainfall—A case study of janina mine, Poland," *Energies*, vol. 15, no. 21, p. 8311, 2022. https://doi.org/10.3390/en15218311

[22] B. Bunda, "Environmental impacts of coal mining at maamba at collieries limited in, Zambia," Dissertations, The University of Zambia, 2001.

[23] C. Phiri, P. Wang, and I. A. Nyambe, "Geology and potential hydrocarbon play system of lower karoo group in the maamba coalfield basin, southern Zambia," *J. Afr. Earth Sci.*, vol. 118, pp. 245–262, 2016. https://doi.org/10.1016/j.jafrearsci.2016.03.006

[24] M. Mtonga, "Technical and environmental aspects of coal mining, a case study on maamba collieries, Zambia," *Zambian J. Appl. Earth Sci.*, vol. 15, 2002.

[25] I. A. Nyambe, "Sedimentology of the gwembe coal formation (permian), lower karoo group, mid-Zambezi valley, southern Zambia," *Fluv. Sedimentol. VI*, pp. 409–434, 1999. https://doi.org/10.1002/9781444304213.ch29

[26] H. Kanno, T. Sakurai, H. Shinjo, H. Miyazaki, Y. Ishimoto, T. Saeki, C. Umetsu, S. Sokotela, and M. Chiboola, "Indigenous climate information and modern meteorological records in sinazongwe district, southern province, Zambia," *Jpn. Agric. Res. Q.*, vol. 47, no. 2, pp. 191–201, 2013. https://doi.org/10.6090/jarq.47.191

[27] T. D. Mitchell and P. D. Jones, "An improved method of constructing a database of monthly climate observations and associated high-resolution grids," *Int. J. Climatol.*, vol. 25, no. 6, pp. 693–712, 2005. https://doi.org/10.1002/joc.1181

[28] B. A. Schrefler and Z. Xiaoyong, "A fully coupled model for water flow and airflow in deformable porous media," *Water Resour. Res.*, vol. 29, no. 1, pp. 155–167, 1993. https://doi.org/10.1029/92WR01737

[29] M. Nuth and L. Laloui, "Effective stress concept in unsaturated soils: Clarification and validation of a unified framework," *Int. J. Numer. Anal. Methods Geomech.*, vol. 32, no. 7, pp. 771–801, 2008. https://doi.org/10.100

2/nag.645

[30] L. Cui and M. Fall, "A coupled thermo–hydro-mechanical–chemical model for underground cemented tailings backfill," *Tunn. Undergr. Space Technol.*, vol. 50, pp. 396–414, 2015. https://doi.org/10.1016/j.tust.2015.08.014

[31] J. Bear, "Dynamics of fluids in porous media," *Soil Sci.*, vol. 120, no. 2, pp. 162–163, 1975. https://doi.org/10.1097/00010694-197508000-00022

[32] M. T. Van Genuchten, "A closed-form equation for predicting the hydraulic conductivity of unsaturated soils," *Soil Sci. Soc. Am. J.*, vol. 44, no. 5, pp. 892–898, 1980. https://doi.org/10.2136/sssaj1980.03615995004400050002x

[33] Y. L. He, L. Z. Yang, and J. Y. Yang, "Governing equations for coupled thermo-hydro-mechanical behaviors in unsaturated rock mass," *J. Southwest Jiaotong Univ.*, vol. 41, pp. 419–423, 2006.

[34] Q. Xu, H. Yin, X. Cao, and Z. Li, "A temperature-driven strength reduction method for slope stability analysis," *Mech. Res. Commun.*, vol. 36, no. 2, pp. 224–231, 2009. https://doi.org/10.1016/j.mechrescom.2008.07.004